Encapsulation of Pb-Free CsSnCl$_3$ Perovskite Nanocrystals with Bone Gelatin: Enhanced Stability and Application in Fe^{3+} Sensing

Dangge Gao,* Ying Zhang, Bin Lyu, Xu Guo, Yelin Hou, Jianzhong Ma,* Bingzhe Yu, and Shaowei Chen*
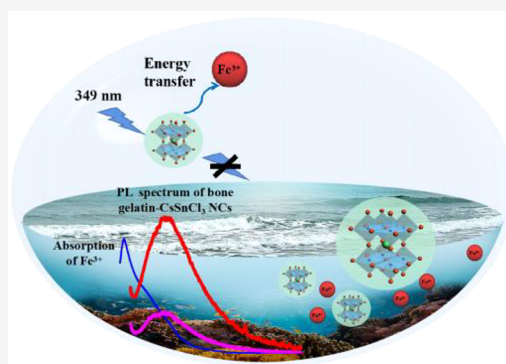
ACCESS | ᵘ Metrics & More | 🞆 Article Recommendations | SI Supporting Information

ABSTRACT: The toxicity of the Pb element limits the large-scale application of inorganic cesium−lead halide (CsPbX$_3$, with X = Cl, Br, and I) perovskite nanocrystals (NCs). Pb-free cesium−tin halide (CsSnX$_3$) NCs have emerged as a viable alternative because of its excellent photoelectric conversion efficiency. However, the applications are hampered by its poor stability and low photoluminescence quantum yield (PLQY). In this study, extraordinarily stable CsSnCl$_3$ NCs were prepared by exploiting bone gelatin as surface capping agents, which retain 95% of the photoluminescence intensity in water for 55 h. Additionally, after bone gelatin encapsulation, the PLQY of CsSnCl$_3$ NCs was found to increase from 2.17% to 3.13% for the uncapped counterparts because of an improved radiative recombination rate. With such remarkable optical properties of the bone gelatin−CsSnCl$_3$ NCs, metal ions like Fe^{3+} in aqueous solutions can be readily detected and monitored, signifying the potential application of such stable bone gelatin−CsSnCl$_3$ NCs in the development of fluorescence sensors and detectors.

1. INTRODUCTION

Perovskite nanocrystals (NCs) are a new kind of functional nanomaterial with a typical chemical formula of ABX$_3$, where A and B represent different metal cations and X refers to anions such as halogen.[1] Inorganic NCs have been widely used in the field of photoelectrics[2] because of their unique optical properties.[3] Current research of NCs is mainly focused on inorganic cesium−lead halide (CsPbX$_3$, with X = Cl, Br, and I) NCs because of their high photoluminescence quantum yield (PLQY),[4] narrow peak width,[5] and ready manipulation of photoluminescence (PL) emission in the entire visible range.[6] However, the Pb element in CsPbX$_3$ NCs may be leached in the form of water-soluble compounds into the environment, posing a threat to the environment and human health.[7] Therefore, it is necessary to develop environmentally benign Pb-free NCs.
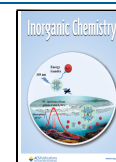
Among these, CsSnX$_3$ NCs are of particular interest thanks to their narrow band gap and low exciton binding energy,[8] with a photoelectric conversion efficiency of up to 14.81%,[9] which is the highest ever reported for Pb-free perovskite solar cells thus far. Therefore, CsSnX$_3$ NCs have been attracting extensive attention as viable alternatives to CsPbX$_3$ NCs in the field of optoelectronics.[10] However, compared with CsPbX$_3$ NCs, CsSnX$_3$ NCs generally exhibit only poor stability, in which Sn^{2+} can be easily converted into Sn^{4+}.[11] Consequently, antioxidants, such as triphenylphosphine[12] and triphenyl oxalate,[13] have been used to impede the oxidation of Sn^{2+}.
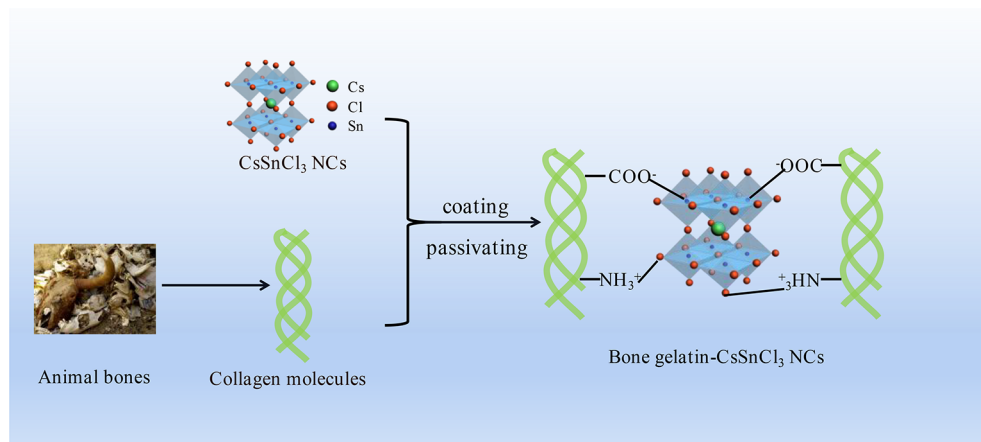
In addition, strong electron-withdrawing groups with large steric hindrance can strongly interact with Sn^{2+} and prevent the destruction of CsSnX$_3$ NCs by water and oxygen. For example, Wang et al.[14] treated CsSnBr$_3$ films with perfluorooctanoic acid (PFOA), and the absorption strength of the films remained unchanged after being placed in air for 16 h. However, materials like PFOA often contain a pungent odor and may have a negative impact on the environment and human health.[15] Furthermore, the materials used to coat NCs are often hydrophobic organics, such as superhydrophobic porous organic polymer frameworks[16] and paraffin,[17] which can reduce the water solubility of NCs and thus limit its application. Therefore, it remains a major challenge to develop new environmentally friendly capping agents that can improve the stability and water solubility of CsSnX$_3$ NCs.

Bone gelatin is a water-soluble polymeric material obtained by the hydrolysis of collagen from animal bones and behaves as a kind of bidentate capping ligand, where the carboxyl and amino groups can strongly chelate to CsSnX$_3$ NCs and effectively improve the stability.[18] In an early study,[11] we

Scheme 1. Schematic Illustration of the Encapsulation of CsSnCl$_3$ NCs by Bone Gelatin

encapsulated CsSnCl$_3$ NCs with gelatin made from waste skin collagen. The obtained material retained 77.46% of the PL intensity after 3 days in water. Both bone gelatin and skin gelatin are natural polymers containing carboxyl, amino, and long molecular chains. The utilization of bone gelatin can enrich the source of capping reagents for NCs stabilization, rendering it possible to further explore their applications, such as fluorescence sensing of transition-metal ions like Fe^{3+}.

Fe^{3+} is an essential trace element in organisms.[19] However, when the content of Fe^{3+} in water exceeds the standard, it will affect the color and smell of water and could enter the human body through the food chain, causing harm to human health and the earth's natural ecological environment.[20] Hence, it is of critical significance to develop effective technologies for the sensitive detection of Fe^{3+} in water. PL-based methods have been attracting immense attention because of their high sensitivity, simplicity, and rapid response. In the past, optical approaches based on organic dyes, such as Rhodamine B, have often been used for Fe^{3+} detection, but their disadvantages are apparent, such as cumbersome functional group modification, low selectivity, and toxicity.[21] In comparison to these conventional organic dyes, NCs possess outstanding properties, in particular, facile sample preparation and adjustable absorption across the optical spectrum, which make NCs an outstanding candidate for the fluorescence detection of Fe^{3+}. Nevertheless, NCs exhibit only poor stability in aqueous media and thus have been mainly used for the detection of nonaqueous substances, such as edible oil[22] and hydrogen sulfide.[23] Thus, it is of both fundamental and technological significance to develop water-soluble NCs such that the detection of Fe^{3+} in water is possible.

In the present study, we describe a facile and low-cost procedure for the effective encapsulation of CsSnCl$_3$ NCs with bone gelatin, where the oxidation of Sn^{2+} to Sn^{4+} was markedly impeded during the growth of NCs. The results showed that the PLQY of bone gelatin−CsSnCl$_3$ NCs was 3.13%, markedly higher than that of the uncapped counterparts (2.17%). Because of the rich hydrophilic carboxyl and amino groups in bone gelatin, the capped CsSnCl$_3$ NCs exhibited good water solubility and, remarkably, also high sensitivity and selectivity in the detection of Fe^{3+} in water based on PL emission.

2. RESULTS AND DISCUSSION

2.1. Synthesis and Morphological Characterization of CsSnCl$_3$ NCs.
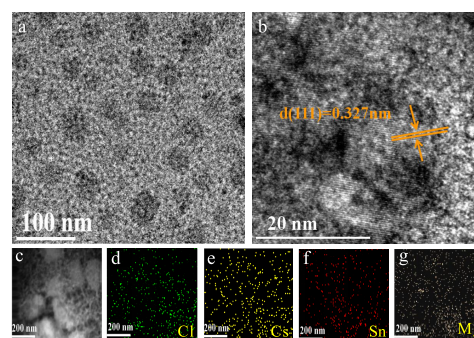As depicted in Scheme 1, bone gelatin was

Figure 1. (a−c) TEM images of bone gelatin−CsSnCl$_3$ NCs and the corresponding EDS-based elemental maps: (d) Cl; (e) Cs; (f) Sn; (g) Mg. The scale bars are (a) 100, (b) 20, and (c−g) 200 nm.

prepared by freeze-drying of animal bone powders treated with acid and alkali, and CsSnCl$_3$ NCs were synthesized separately via a thermal procedure with Cs$_2$CO$_3$ and SnCl$_2$ in a nitrogen atmosphere.[11] Bone gelatin−CsSnCl$_3$ NCs were obtained by mixing bone gelatin and CsSnCl$_3$ NCs in glycerol at ambient temperature (details are given in the Supporting Information). From the Fourier transform infrared (FTIR) spectrum in Figure S1, the obtained bone gelatin can be seen to display several major vibrational bands at 1650, 1550, and 1230 cm^{-1}, which are characteristic of amides I (C═O stretch), II (N−H bending), and III (C−O stretching), respectively, indicating the formation of a special triple-helix conformation.[24] The morphology of bone gelatin was then characterized by scanning electron microscopy (SEM) measurements. Figure S2a depicts a representative SEM image of bone gelatin, which exhibited a lamellar structure and a somewhat rough surface. Gel permeation chromatography (GPC) measurements (Figure S2b) showed a rather narrow relative molecular weight distribution, suggesting high purity and a relatively monodisperse composition. As shown in Table S1, the number-average (M_n) and weight-average (M_w) molecular weights of the obtained bone gelatin were 37 675 and 138 808 Da, respectively.

The dimensions and morphology of the CsSnCl$_3$ NCs and bone gelatin−CsSnCl$_3$ NCs were first examined and compared by transmission electron microscopy (TEM) measurements. In Figure S3, we can see that the CsSnCl$_3$ NCs exhibited a cubic shape with an average size of 25 ± 5 nm. After bone gelatin coating, the average size of the CsSnCl$_3$ NCs reached 38 ± 3
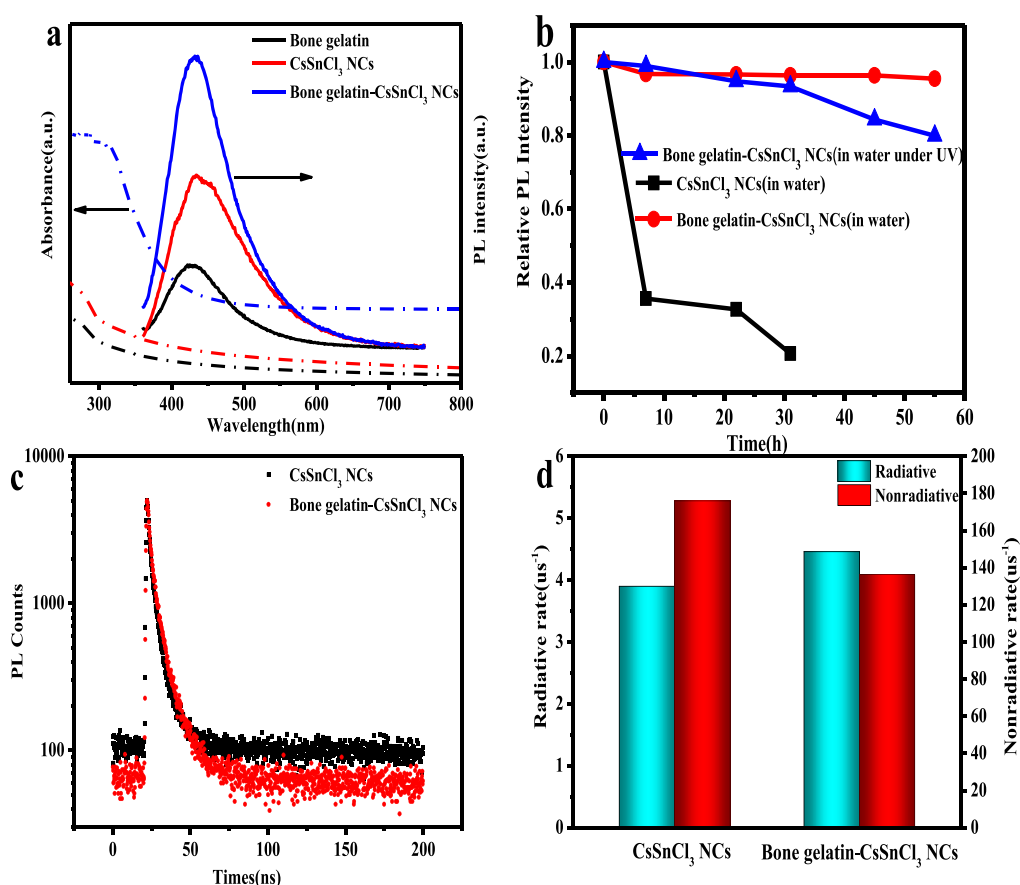
Figure 2. (a) UV−vis absorption (dash-dotted) and PL emission (solid) curves of bone gelatin, $CsSnCl_3$ NCs, and bone gelatin−$CsSnCl_3$ NCs. The PL emission curves were acquired upon excitation at 349 nm. (b) Time-resolved PL intensity of uncapped and bone gelatin−$CsSnCl_3$ NCs in air and under UV radiation. (c) Time-resolved PL decays of uncapped and bone gelatin−capped $CsSnCl_3$ NCs. (d) Histograms of the radiative and nonradiative recombination rates for uncapped and bone gelatin−$CsSnCl_3$ NCs.

Table 1. τ_{av} and PLQY Values of Bone Gelatin- $CsSnCl_3$ NCs and Relevant Pb-Free Perovskites

sample	τ_{av} (ns)	PLQY (%)	ref
bone gelatin−$CsSnCl_3$ NCs	7.11	3.13	this work
skin gelatin−$CsSnCl_3$ NCs	8.84		11
$CsSnCl_3$ NCs	2.14	0.17	13
$CsSnBr_3$ nanowires	1.1		26
$CsSnBr_3$ cubic nanocages	6.52	2.1	14
$AgBiI_4$ quantum dots	4.6	4	27

nm. From the high-resolution TEM image in Figure 1b, well-defined lattice fringes can be seen with an interplanar spacing of 0.327 nm, corresponding to the (111) surfaces of the $CsSnCl_3$ NCs in Figure S3b (JCPDS 74-2058). Additionally, energy-dispersive spectroscopy (EDS)-based elemental mapping analysis (Figure 1c−g) showed that the elements of Cl, Cs, and Sn were enriched within the dark regions of the bright-field TEM image, whereas the element Mg in bone gelatin was distributed rather evenly across the sample. Among them, the Mg element came from bone gelatin and the Cl, Cs, and Sn elements came from the $CsSnCl_3$ NCs, suggesting uniform encapsulation of the $CsSnCl_3$ NCs within bone gelatin.

2.2. Optical Properties and Stability Characterization. Encapsulation of $CsSnCl_3$ NCs with bone gelatin led to a marked variation of the optical properties. The PL emission and absorption spectra of bone gelatin, as-prepared $CsSnCl_3$ NCs, and bone gelatin−$CsSnCl_3$ NCs are shown in Figure 2a.
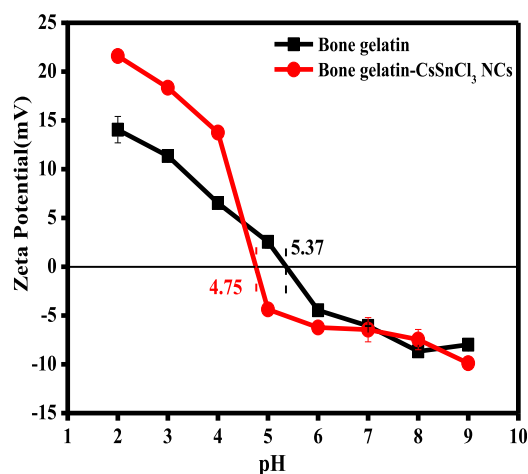

Figure 3. ζ potential of bone gelatin−$CsSnCl_3$ NCs and bone gelatin.

The as-prepared $CsSnCl_3$ NCs dispersed in cyclohexane exhibited a characteristic absorption peak at 349 nm and an emission maximum (λ_{em}) at 436 nm. Such absorption and emission characteristics were retained after bone gelatin coating, indicating that bone gelatin did not introduce distortion in the band energy of the $CsSnCl_3$ NCs. However, the (normalized) emission intensity of bone gelatin−$CsSnCl_3$ NCs was markedly higher than the sum of bone gelatin and $CsSnCl_3$ NCs. This is likely because the long molecular chains
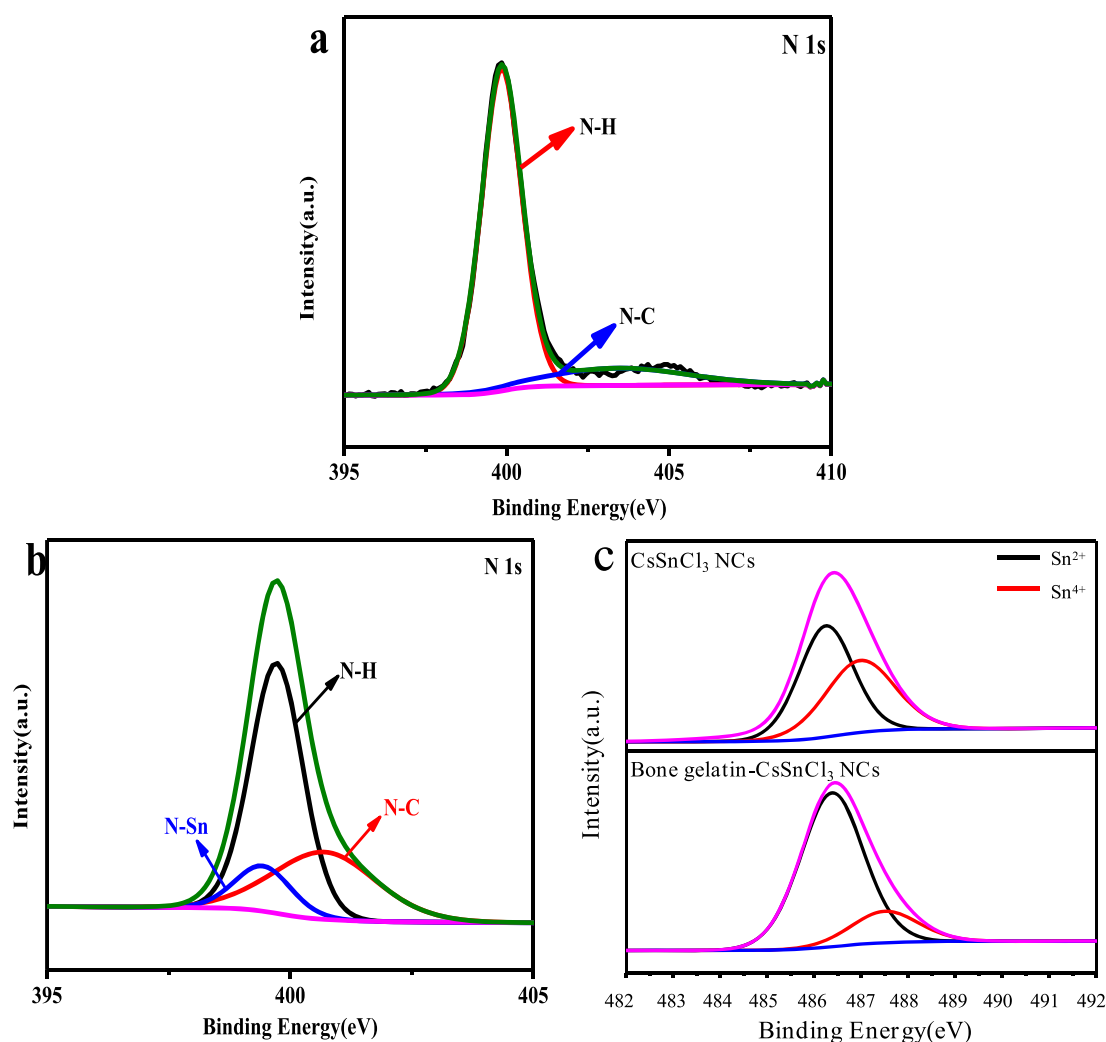
Figure 4. N 1s XPS spectra of (a) bone gelatin and (b) bone gelatin−$CsSnCl_3$ NCs. (c) Sn $3d_{5/2}$ XPS spectra of bone gelatin−$CsSnCl_3$ NCs and $CsSnCl_3$ NCs.

of bone gelatin facilitate the effective encapsulation of $CsSnCl_3$ NCs and reduce the surface defects, thus enhancing the fluorescence emission of $CsSnCl_3$ NCs.

It is well-known that the Sn^{2+} of $CsSnCl_3$ NCs can be easily oxidized to Sn^{4+} under ambient conditions, which compromises the material structural stability. Therefore, we compared the stability of $CsSnCl_3$ NCs with and without bone gelatin encapsulation in water and under photoirradiation. Figure 2b shows the variation of the PL emission intensity of $CsSnCl_3$ NCs with and without bone gelatin capping dispersed in water for up to 60 h. It can be seen that only 35% of the initial PL intensity was retained with the uncapped $CsSnCl_3$ NCs in water after only 7 h. By sharp contrast, the bone gelatin−$CsSnCl_3$ NCs remained at 95% of the PL intensity after being dispersed in water for 55 h (Figure 2b). Note that the latter is also markedly higher than that of skin gelatin−$CsSnCl_3$ NCs reported previously (80% retention after 48 h),[11] most likely because of the high carboxyl content in bone gelatin compared to that in skin gelatin (Table S2), considering that the carboxyl moiety is the point of anchor on the NCs.[25]

Figure 2c shows the normalized PL emission decay profiles of $CsSnCl_3$ NCs with and without bone gelatin encapsulation. After bone gelatin modification, the PLQY of $CsSnCl_3$ NCs was found to increase from 2.17% to 3.13% and the average

fluorescent lifetime (τ_{av}) increased from 5.56 to 7.11 ns. As can be seen from Table 1, τ_{av} and PLQY of the bone gelatin−$CsSnCl_3$ NCs were even higher than those of other Pb-free NCs reported in the literature. This suggests a reduced content of structural defects (trap states) within the NCs after surface functionalization with bone gelatin.

Figure 2d shows the radiative (Γ_{rad}) and nonradiative (Γ_{nonrad}) recombination rates for $CsSnCl_3$ NCs with and without bone gelatin encapsulation, which are estimated by the following equations:[10]

$$\Gamma_{rad} = \frac{PLQY}{\tau_{av}} \tag{1}$$

$$\Gamma_{nonrad} = \frac{1 - PLQY}{\tau_{av}} \tag{2}$$

Obviously, after bone gelatin coating, the nonradiation recombination rate of $CsSnCl_3$ NCs decreased from 175.95 to 136.25 μs^{-1}, whereas the radiation recombination rate increased from 3.90 to 4.46 μs^{-1}. This suggests that bone gelatin effectively stabilized the excited state by suppressing the formation of nonradiative recombination pathways.

ζ-potential analysis (Figure 3) shows that the isoelectric point (pI) of bone gelatin was 5.37, which decreased somewhat
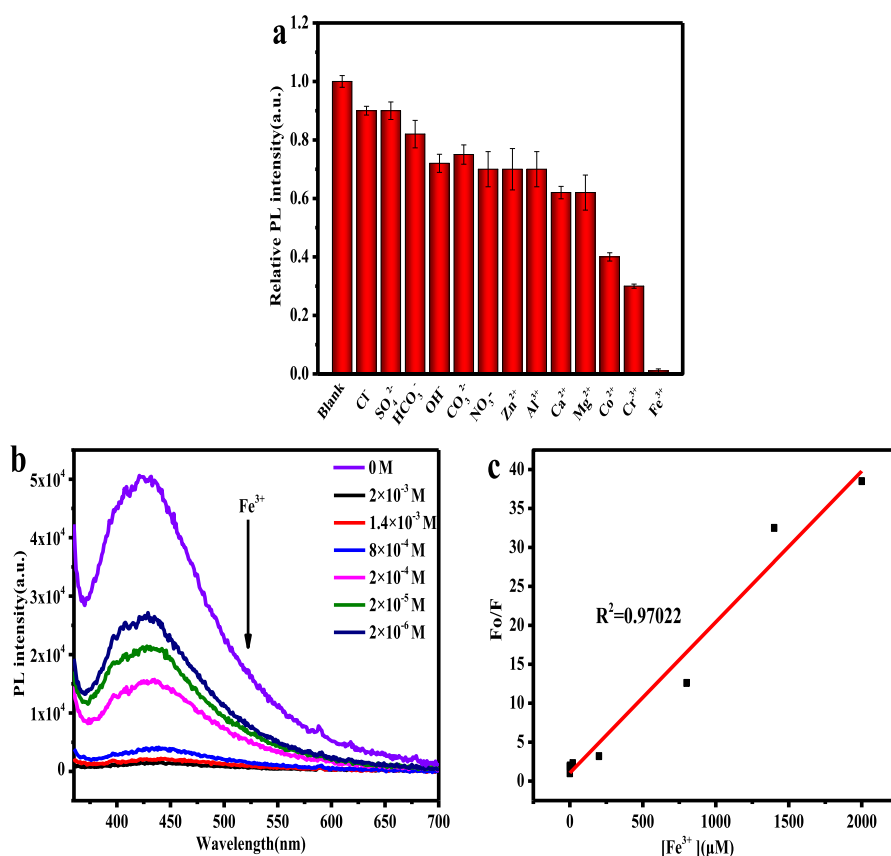
Figure 5. (a) PL emission intensity at 349 nm of bone gelatin−CsSnCl$_3$ NCs with the addition of a range of cations and anions at a concentration of 0.2 mM. (b) PL emission spectra of bonegelatin- CsSnCl$_3$ NCs with the addition of Fe^{3+} ions at various concentrations. (c) Stern−Volmer plots for the F_0/F values and different Fe^{3+} ion concentrations.
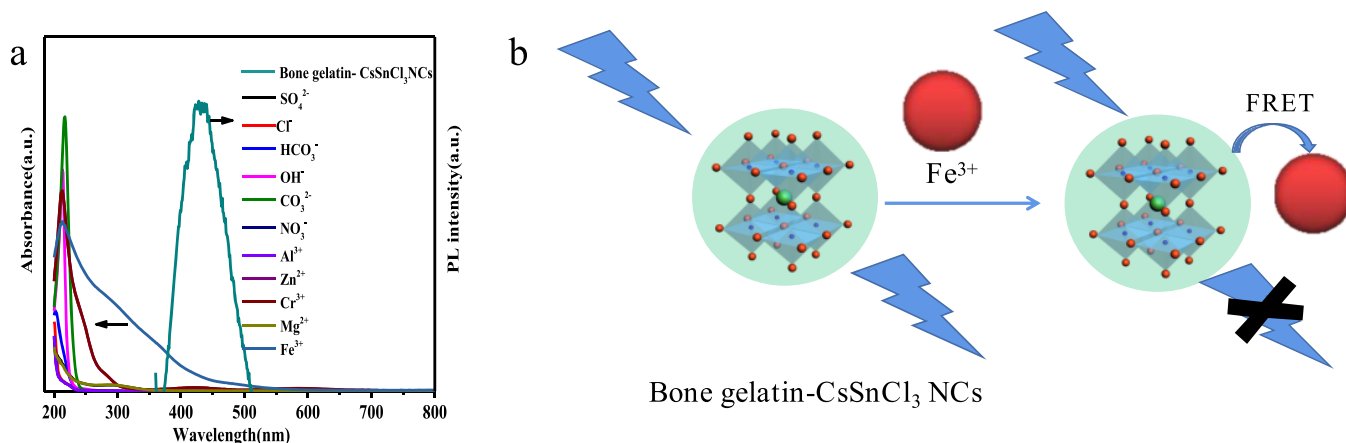

Figure 6. (a) PL emission spectrum of bone gelatin−CsSnCl$_3$ NCs and absorption spectra with the addition of different ions (0.2 mM) in aqueous solution. (b) Diagram of the detection mechanism of bone gelatin−CsSnCl$_3$ NCs for Fe^{3+} ions.

to 4.75 with bone gelatin- CsSnCl$_3$ NCs. Note that bone gelatin is an amphoteric electrolyte, where the pI is related to the ratio of the −COOH to −NH$_2$ moieties.[28] In the bone gelatin−CsSnCl$_3$ NCs, it is likely that the −COO$^-$ groups bind to Sn^{2+}, which promoted the ionization of −COOH and led to a decreased pI.

X-ray photoelectron spectroscopy (XPS) measurements were then carried out to analyze the surface chemical composition and valence states of the samples. Figure S4a shows the peaks of C 1s, N 1s, and O 1s in bone gelatin. From the survey spectrum in Figure S4b, the elements of C 1s, N 1s,

O 1s, Cs 3s, Sn 3d, and Cl 2p can be clearly resolved. It can be seen from the fitting peaks of N 1s in Figure 4b that, in addition to the N−H peak at 399.6 eV and the N−C peak at 400.8 eV in bone gelatin (Figure 4a), there was also a Sn−N peak at 399.9 eV.[11] This suggests that encapsulation of the CsSnCl$_3$ NCs was due to coordination of the −NH$_2$ of bone gelatin to the Sn^{2+} centers in the NCs. The content of Sn^{4+} in CsSnCl$_3$ NCs and bone gelatin−CsSnCl$_3$ NCs was determined by deconvolution of the XPS spectra of Sn 3d$_{5/2}$.[29] Both CsSnCl$_3$ NCs and bone gelatin−CsSnCl$_3$ NCs were determined after 2 days of exposure to oxygen. As shown in

Figure 4c, the Sn^{4+} content was considerably lower in bone gelatin−$CsSnCl_3$ NCs, indicating greatly suppressed Sn^{2+} oxidation. This is because the protective effect of bone gelatin increases the antioxidant capacity of $CsSnCl_3$ NCs.

2.3. Fe^{3+} Ion Sensing. With their good water stability and antioxidant capacity, bone gelatin- $CsSnCl_3$ NCs displayed great potential as a PL sensor for metal ions in aqueous media. From Figure 5a, we can see that the PL emission intensity at 349 nm of bone gelatin−$CsSnCl_3$ NCs in water diminished somewhat upon the addition of a range of metal cations and anions at a concentration of 0.2 mM, such as Cl^-, SO_4^{2-}, HCO_3^-, NO_3^-, OH^-, Zn^{2+}, Al^{3+}, Ca^{2+}, Mg^{2+}, and Co^{2+}, and was almost completely quenched by Fe^{3+}. This suggests that bone gelatin- $CsSnCl_3$ NCs may serve as a unique sensing platform for Fe^{3+}.

As shown in Figure 5b, with an increase of the Fe^{3+} concentrations, the PL intensity of bone gelatin- $CsSnCl_3$ NCs decreased accordingly, which can be fitted by the Stern−Volmer equation[30]

$$F_0/F = 1 + K_{sv}[C] \tag{3}$$

where F_0 and F represent the PL emission intensities of the bone gelatin−$CsSnCl_3$ NCs in the absence and presence of a Fe^{3+} ion, respectively, $[C]$ is the concentration of Fe^{3+}, and K_{sv} is a Stern−Volmer constant. Linear regression yields the relationship $F_0/F = 0.735 + 4.609[C]$, with a correlation coefficient (R^2) of 0.97022 and a quenching constant (K_{sv}) of 4.6×10^3 M^{-1}. The calibration curve shows the linear ranges from 0 to 2000 μM, and the limit of detection was calculated to be 8 μM (S/N = 3).

The PL spectrum of bone gelatin- $CsSnCl_3$ NCs and the absorption spectra upon the addition of different ions (0.2 mM) in aqueous solution are shown in Figure 6a. Compared with other ions, only the absorption spectrum of Fe^{3+} overlapped significantly with the emission profile of the bone-gelatin-capped $CsSnCl_3$ NCs, suggesting that quenching of the PL emission was due to fluorescence resonance energy transfer (FRET).[25] A mechanism of action between bone-gelatin- $CsSnCl_3$ NCs and Fe^{3+} was proposed and is shown in Figure 6b, where bone gelatin−$CsSnCl_3$ NCs and Fe^{3+} serve as the energy donor and acceptor, respectively. In the absence of Fe^{3+}, bone gelatin−$CsSnCl_3$ NCs will fluoresce once the electrons in the NCs are excited and radiation transition occurs. In the presence of sufficient Fe^{3+}, the energy of bone gelatin−$CsSnCl_3$ NCs is transferred to Fe^{3+}, which inhibits its radiation transition and causes fluorescence quenching of the NCs.

3. CONCLUSIONS

In summary, highly stable bone gelatin−$CsSnCl_3$ NCs were prepared by the simple mixing of bone gelatin and $CsSnCl_3$ NCs. This is most likely due to the −COOH and −NH_2 moieties in bone gelatin that effectively passivate the surface defects of $CsSnCl_3$ NCs. The long molecular chains of bone gelatin helped to facilitate the encapsulation of $CsSnCl_3$ NCs within the polymer matrix and inhibit the degradation and oxidation of $CsSnCl_3$ NCs in water or under photoirradiation. Notably, with bone gelatin encapsulation, the $CsSnCl_3$ NCs showed a higher PLQY and longer τ_{av} than the uncapped counterparts. The excellent water stability and PL emissive properties of the bone gelatin-passivated NCs could be exploited as fluorescence probes to monitor Fe^{3+} in aqueous solution, likely because of FRET.

■ ASSOCIATED CONTENT

ⓈⒾ Supporting Information

The Supporting Information is available free of charge at https://pubs.acs.org/doi/10.1021/acs.inorgchem.2c00354.

Experimental details, FTIR and XPS spectra, SEM and TEM images, GPC curve, carboxyl and amino group contents, and molecular weights (PDF)

■ AUTHOR INFORMATION

Corresponding Authors

Dangge Gao − *College of Bioresources Chemical and Materials Engineering and Key Laboratory of Auxiliary Chemistry and Technology for Chemical Industry, Shaanxi University of Science and Technology, Xi'an, Shaanxi 710021, China; Xi'an Key Laboratory of Green Chemicals and Functional Materials, Xi'an, Shaanxi 710021, China;* ⓞ orcid.org/0000-0002-9100-4917; Email: dangge2000@126.com

Jianzhong Ma − *College of Bioresources Chemical and Materials Engineering and Key Laboratory of Auxiliary Chemistry and Technology for Chemical Industry, Shaanxi University of Science and Technology, Xi'an, Shaanxi 710021, China; Xi'an Key Laboratory of Green Chemicals and Functional Materials, Xi'an, Shaanxi 710021, China;* ⓞ orcid.org/0000-0003-0512-702X; Email: majz@sust.edu.cn

Shaowei Chen − *Department of Chemistry and Biochemistry, University of California, Santa Cruz, California 96064, United States;* ⓞ orcid.org/0000-0002-3668-8551; Email: shaowei@ucsc.edu

Authors

Ying Zhang − *College of Bioresources Chemical and Materials Engineering and Key Laboratory of Auxiliary Chemistry and Technology for Chemical Industry, Shaanxi University of Science and Technology, Xi'an, Shaanxi 710021, China; Xi'an Key Laboratory of Green Chemicals and Functional Materials, Xi'an, Shaanxi 710021, China*

Bin Lyu − *College of Bioresources Chemical and Materials Engineering and Key Laboratory of Auxiliary Chemistry and Technology for Chemical Industry, Shaanxi University of Science and Technology, Xi'an, Shaanxi 710021, China; Xi'an Key Laboratory of Green Chemicals and Functional Materials, Xi'an, Shaanxi 710021, China;* ⓞ orcid.org/0000-0001-8785-2246

Xu Guo − *College of Bioresources Chemical and Materials Engineering and Key Laboratory of Auxiliary Chemistry and Technology for Chemical Industry, Shaanxi University of Science and Technology, Xi'an, Shaanxi 710021, China; Xi'an Key Laboratory of Green Chemicals and Functional Materials, Xi'an, Shaanxi 710021, China*

Yelin Hou − *College of Bioresources Chemical and Materials Engineering and Key Laboratory of Auxiliary Chemistry and Technology for Chemical Industry, Shaanxi University of Science and Technology, Xi'an, Shaanxi 710021, China; Xi'an Key Laboratory of Green Chemicals and Functional Materials, Xi'an, Shaanxi 710021, China*

Bingzhe Yu − *Department of Chemistry and Biochemistry, University of California, Santa Cruz, California 96064, United States*

Complete contact information is available at:
https://pubs.acs.org/10.1021/acs.inorgchem.2c00354

■ REFERENCES

(1) Lv, W. Z.; Li, L.; Xu, M. C.; Hong, J. X.; Tang, X. X.; Xu, L. G.; Wu, Y. H.; Zhu, R.; Chen, R. F.; Huang, W. Improving the Stability of Metal Halide Perovskite Quantum Dots by Encapsulation. *Adv. Mater.* **2019**, *31*, 1900682.

(2) Wang, Y.; Yuan, J. Y.; Zhang, X. L.; Ling, X. F.; Larson, B. W.; Zhao, Q.; Yang, Y. G.; Shi, Y.; Luther, J. M.; Ma, W. L. Surface Ligand Management Aided by a Secondary Amine Enables Increased Synthesis Yield of CsPbI$_3$ Perovskite Quantum Dots and High Photovoltaic Performance. *Adv. Mater.* **2020**, *32*, 2000449.

(3) Liang, S.; Zhang, M.; Biesold, G. M.; Choi, W.; He, Y.j.; Li, Z.l.; Shen, D. F.; Lin, Z. Recent Advances in Synthesis, Properties, and Applications of Metal Halide Perovskite Nanocrystals/Polymer Nanocomposites. *Adv. Mater.* **2021**, *33*, 2005888.

(4) He, Y.; Liang, Y.; Liang, S.; Harn, Y. W.; Li, Z.; Zhang, M.; et al. Dual-Protected Metal Halide Perovskite Nanosheets with an Enhanced Set of Stabilities. *Angew. Chem., Int. Ed.* **2021**, *133*, 7335−7342.

(5) Gong, M. G.; Sakidja, R.; Goul, R.; Ewing, D.; Casper, M.; Stramel, A.; Elliot, A.; Wu, J. Z. High-Performance All-Inorganic CsPbCl$_3$ Perovskite Nanocrystal Photodetectors with Superior Stability. *ACS Nano* **2019**, *13*, 1772−1783.

(6) Dutta, A.; Behera, R. K.; Pal, P.; Baitalik, S.; Pradhan, N. Near-Unity Photoluminescence Quantum Efficiency for All CsPbX$_3$ (X = Cl, Br, and I) Perovskite Nanocrystals: A Generic Synthesis Approach. *Angew. Chem., Int. Ed.* **2019**, *58*, 5552−5556.

(7) Infante, I.; Manna, L. Are There Good Alternatives to Lead Halide Perovskite Nanocrystals? *Nano Lett.* **2021**, *21*, 6−9.

(8) Ma, L.; Hao, F.; Stoumpos, C. C.; Phelan, B. T.; Wasielewski, M. R.; Kanatzidis, M. G. Carrier Diffusion Lengths of over 500 nm in Lead-Free Perovskite CH$_3$NH$_3$SnI$_3$ Films. *J. Am. Chem. Soc.* **2016**, *138*, 14750−14755.

(9) Yu, B. B.; Chen, Z. H.; Zhu, Y. D.; Wang, Y. R.; Han, B.; Chen, G. C.; Zhang, X. S.; Du, J.; He, Z. B. Heterogeneous 2D/3D Tin-Halides Perovskite Solar Cells with Certified Conversion Efficiency Breaking 14%. *Adv. Mater.* **2021**, *33*, 2102055.

(10) Liu, Q.; Yin, J.; Zhang, B. B.; Chen, J. K.; Zhou, Y.; Zhang, L. M.; Wang, L. M.; Zhao, Q.; Hou, J. S.; Shu, J.; Song, B.; Shirahata, N.; Bakr, O. M.; Mohammed, O. F.; Sun, H. T. Theory-Guided Synthesis of Highly Luminescent Colloidal Cesium Tin Halide Perovskite Nanocrystals. *J. Am. Chem. Soc.* **2021**, *143*, 5470−5480.

(11) Lyu, B.; Guo, X.; Gao, D. G.; Kou, M. N.; Yu, Y. J.; Ma, J. Z.; Chen, S. W.; Wang, H.; Zhang, Y.; Bao, X. Highly-Stable Tin-Based Perovskite Nanocrystals Produced by Passivation and Coating of Gelatin. *J. Hazard Mater.* **2021**, *403*, 123967.

(12) Wang, Y. Y.; Tu, J.; Li, T. H.; Tao, C.; Deng, X. Y.; Li, Z. Convenient Preparation of CsSnI$_3$ Quantum Dots, Excellent Stability, and the Highest Performance of Lead-Free Inorganic Perovskite Solar Cells So Far. *J. Mater. Chem. A* **2019**, *7*, 7683−7690.

(13) Kang, C. T.; Rao, H. S.; Fang, Y. P.; Zeng, J. J.; Pan, Z. X.; Zhong, X. H. Antioxidative Stannous Oxalate Derived Lead-Free Stable CsSnX$_3$ (X = Cl, Br, and I) Perovskite Nanocrystals. *Angew. Chem., Int. Ed.* **2021**, *60*, 660−665.

(14) Wang, A. F.; Guo, Y. Y.; Muhammad, F.; Deng, Z. T. Controlled Synthesis of Lead-Free Cesium Tin Halide Perovskite Cubic Nanocages with High Stability. *Chem. Mater.* **2017**, *29*, 6493−6501.

(15) Ding, W. H.; Tan, X. J.; Chen, G. H.; Xu, J. Y.; Yu, K.; Huang, Y. X. Molecular-Level Insights on the Facet-Dependent Degradation of Perfluorooctanoic Acid. *ACS Appl. Mater. Interfaces* **2021**, *13*, 41584−41592.

(16) Xuan, T. T.; Huang, J. J.; Liu, H.; Lou, S. Q.; Cao, L. Y.; Gan, W. J.; Liu, R. S.; Wang, J. Super-Hydrophobic Cesium Lead Halide Perovskite Quantum Dot-Polymer Composites with High Stability and Luminescent Efficiency for Wide Color Gamut White Light-Emitting Diodes. *Chem. Mater.* **2019**, *31*, 1042−1047.

(17) Wu, H. S.; Lin, S.; Wang, R. N.; You, X.; Chi, Y. W. Water-Stable and Ion Exchange-Free Inorganic Perovskite Quantum Dots Encapsulated in Solid Paraffin and Their Application in Light Emitting Diodes. *Nanoscale* **2019**, *11*, 5557−5563.

(18) Xue, Z. P.; Gao, H.; Liu, W. J.; Li, X. L. Facile Room-Temperature Synthesis of High-Chemical-Stability Nitrogen-Doped Graphene Quantum Dot/CsPbBr$_3$ Composite. *ACS Appl. Electron. Mater.* **2019**, *1*, 2244−2252.

(19) Qiang, R. B.; Sun, W. M.; Hou, K. M.; Li, Z. P.; Zhang, J. Y.; Ding, Y.; Wang, J. Q.; Yang, S. R. Electrochemical Trimming of Graphene Oxide Affords Graphene Quantum Dots for Fe^{3+} Detection. *ACS Appl. Nano Mater.* **2021**, *4*, 5220−5229.

(20) Jornet-Molla, V.; Dreessen, C.; Romero, F. M. Robust Lanthanoid Picolinate-Based Coordination Polymers for Luminescence and Sensing Applications. *Inorg. Chem.* **2021**, *60*, 10572−10584.

(21) Guo, R. H.; Zhou, S. X.; Li, Y. C.; Li, X. H.; Fan, L. Z.; Voelcker, N. H. Rhodamine-Functionalized Graphene Quantum Dots for Detection of Fe^{3+} in Cancer Stem Cells. *ACS Appl. Mater. Interfaces* **2015**, *7*, 23958−23966.

(22) Zhao, Y.; Xu, Y. J.; Shi, L. X.; Fan, Y. Perovskite Nanomaterial-Engineered Multiplex-Mode Fluorescence Sensing of Edible Oil Quality. *Anal. Chem.* **2021**, *93*, 11033−11042.

(23) Chen, C. Q.; Cai, Q.; Luo, F.; Dong, N.; Guo, L. H.; Qiu, B.; Lin, Z. Y. Sensitive Fluorescent Sensor for Hydrogen Sulfide in Rat Brain Microdialysis via CsPbBr$_3$ Quantum Dots. *Anal. Chem.* **2019**, *91*, 15915−15921.

(24) Gao, D. G.; Wang, P. P.; Shi, J. B.; Li, F.; Li, W. B.; Lyu, B.; Ma, J. Z. A Green Chemistry Approach to Leather Tanning Process: Cage-Like Octa(Aminosilsesquioxane) Combined with Tetrakis-(hydroxymethyl) Phosphonium Sulfate. *J. Clean. Prod.* **2019**, *229*, 1102−1111.

(25) Pan, A. Z.; He, B.; Fan, X. Y.; Liu, Z. K.; Urban, J. J.; Alivisatos, A. P.; He, L.; Liu, Y. Insight into the Ligand-Mediated Synthesis of Colloidal CsPbBr$_3$ Perovskite Nanocrystals: The Role of Organic Acid, Base, and Cesium Precursors. *ACS Nano* **2016**, *10*, 7943−7954.

(26) Chen, J.; Luo, Z. Y.; Fu, Y. P.; Wang, X. X.; Czech, K. J.; Shen, S. S.; Guo, L. J.; Wright, J. C.; Pan, A. L.; Jin, S. Tin(IV)-Tolerant Vapor-Phase Growth and Photophysical Properties of Aligned Cesium Tin Halide Perovskite (CsSnX$_3$; X = Br, I) Nanowires. *ACS Energy Lett.* **2019**, *4*, 1045−1052.

(27) Premkumar, S.; Liu, D.; Zhang, Y. M.; Nataraj, D.; Ramya, S.; Jin, Z. Z.; Mamba, B. B.; Kuvarega, A. T.; Gui, J. Z. Stable Lead-Free Silver Bismuth Iodide Perovskite Quantum Dots for UV Photodetection. *ACS Appl. Nano Mater.* **2020**, *3*, 9141−9150.

(28) Nadendla, K.; Friedman, S. H. Light Control of Protein Solubility Through Isoelectric Point Modulation. *J. Am. Chem. Soc.* **2017**, *139*, 17861−17869.

(29) Zhang, T.; Li, H.; Ban, H. X.; Sun, Q.; Shen, Y.; Wang, M. K. Efficient CsSnI$_3$-Based Inorganic Perovskite Solar Cells Based on A Mesoscopic Metal Oxide Framework via Incorporating A Donor Element. *J. Mater. Chem. A* **2020**, *8*, 4118−4124.

(30) Pramata, A. D.; Akaishi, Y.; Kodama, N.; Mokuge, Y.; Kawashima, S.; Shimoyoshi, M.; Sairot, C.; Nuket, P.; Vas-Umnuay, P.; Kida, T. TiO$_2$-Coated CsPbI$_3$ Quantum Dots Coupled with

Polyoxometalates for On/Off Fluorescent Photoswitches. *ACS Appl. Nano Mater.* **2021**, *4*, 4103−4113.